

Combining Topological and Geometrical Features for Global and Partial 3-D Shape Retrieval

Athanasios Mademlis, Petros Daras, *Member, IEEE*, Apostolos Axenopoulos, Dimitrios Tzovaras, and Michael G. Strintzis, *Fellow, IEEE*

Abstract—This paper presents a novel framework for 3-D object content-based search and retrieval, appropriate for both partial and global matching applications. The framework is based on a graph representation of a 3-D object which is enhanced by local geometric features. The 3-D object is decomposed into meaningful parts and an attributed graph is constructed based on the connectivity of the parts. Every 3-D part is approximated with a suitable superellipsoid and a novel 3-D shape descriptor, called a 3-D distance field descriptor, is computed and associated to the corresponding graph nodes. The matching process used is based on attributed graph matching algorithm appropriate for this application. The proposed method not only provides successful retrieval results in terms of geometric similarity but also is invariant to rotation, translation and scaling of an object as well as to the different poses of articulated objects. Finally, it can be effectively used for partial and global 3-D object retrieval.

Index Terms—3-D shape retrieval, global matching, partial matching, topological matching.

I. INTRODUCTION

THREE-DIMENSIONAL (3-D) shape matching has evolved to a very promising research area during the last years. At the same time, a variety of emerging applications (e.g., CAD, games design, computer animations, and molecular biology) dictates the need for efficient 3-D search and retrieval tools. Among the several approaches introduced for 3-D shape matching, the most well-known are based on low-level global geometrical features, which can be extracted from the global shape of a 3-D object [1]. Others are mainly based on topological features and attempt to produce a skeletal representation of an object and utilize skeletal graph-matching techniques for similarity comparisons [1]. In order to exploit benefits from both aforementioned categories of methods, new approaches are needed that will rely equally on geometrical and topological information. Further, a new challenge in this research field is the partial matching, which is a very important prerequisite in search and retrieval of 3-D objects acquired from 3-D scenes.

Manuscript received January 11, 2008; revised November 28, 2007. First published June 3, 2008; last published July 9, 2008 (projected). This work was supported by the VICTORY and CATER EC IST projects, by the altaB23D Greek project and by the PENED 03E Δ 36 project co-financed 75% by the European Union and 25% by the Greek Secretariat for Research and Technology. The associate editor coordinating the review of this manuscript and approving it for publication was Dr. Wen Gao.

A. Mademlis and M. G. Strintzis are with the Department of Electrical and Computer Engineering, Aristotle University of Thessaloniki, 54006, Thessaloniki, Greece (e-mail: mademlis@iti.gr; strintzi@eng.auth.gr).

P. Daras, A. Axenopoulos, and D. Tzovaras are with the Informatics and Telematics Institute, GR-570 01 Themi, Thessaloniki, Greece (e-mail: daras@iti.gr; axenop@iti.gr; Dimitrios.Tzovaras@iti.gr).

Digital Object Identifier 10.1109/TMM.2008.922790

A. Background and Related Work

1) *Geometry-Based Approaches*: In the area of 3-D content-based search and retrieval, a variety of methods have been proposed so far. These methods are based on global geometrical features of 3-D models, which can be extracted either from their surface or from their volumetric representation. In [5], a fast querying-by-3D-model approach, is presented, where the descriptors are chosen so as to mimic the basic criteria that humans use for the same purpose. In [6], a 3-D search and retrieval method based on the generalized radon transform (GRT) is proposed where two forms of the GRT are presented. In [10], an approach that measures the similarity among 3-D models by visual similarity is proposed. In [11] and [12], a method where the descriptor vector is obtained by forming a complex function on the sphere is presented. Then, spherical harmonics are obtained which form the rotation invariant descriptor vector.

In [19], the MPEG-7 shape spectrum descriptor is defined as the histogram of the shape index, calculated over the entire surface of a 3-D object and is invariant under rotation, translation and scaling. In [18], the Spherical Harmonic Representation is presented which transforms rotation dependent descriptors into rotation invariant ones. Novotni and Klein applied and extended Canterakis' [13] theoretical framework for 3-D Zernike moments in [20]. These are computed as a projection of the function which defines the object onto a set of orthonormal functions within the unit ball.

2) *Topology-Based Approaches*: Most of the methods for 3-D content-based search described above have shown remarkable performance in a broad range of applications. However, the fact that these techniques are applied to the global shape of a 3-D object makes them inappropriate to be used in the cases where the articulation transformations of 3-D objects are of crucial importance, or the partial matching is the main objective. Global shape approaches describe the whole object using a feature vector. Any articulation change, or a missing part of the object, will result in a completely different feature vector, which cannot be used for 3-D object retrieval. Thus, a part-based representation of the object where the feature vectors will be extracted for each part is needed. Several approaches have been proposed regarding the decomposition of a 3-D object into a set of connected segments. Some of them are focusing on finding special features in triangulated meshes, such as salient points or curvature information, in order to decompose the mesh into a set of meaningful parts. Others are based on skeleton extraction, by appropriately thinning a 3-D object. A brief overview of the most representative methods is given in the sequel.

In [14] a technique, called Topology Matching, is introduced, which calculates the similarity between polyhedral models by

comparing multiresolutional Reeb graphs (MRGs). Based on the idea of MRG matching [14], Chen *et al.* [15] propose a 3-D model retrieval system, where a preprocessing step has been added before the Reeb Graph extraction in order to accelerate the graph-matching and retrieval processes. The work in [14] has been further extended in [16], where the Reeb graph is augmented with geometrical attributes leading to the creation of a flexible multiresolutional representation, called an augmented Reeb graph.

In [17], a hierarchical mesh decomposition algorithm is proposed. The algorithm computes a 3-D object mesh decomposition, which generally refers to segmentation at regions of deep concavities. In [23], an automated algorithm for decomposing complex objects is presented, which is based on salient feature extraction and curvature estimation. For each segment of the object, rotation invariant geometrical descriptors are extracted and used for classification.

Several approaches have been introduced for skeletal graph extraction and matching. An approach for the search and retrieval of engineering objects has been proposed by Iyer and Lou [2]–[4]. The matching is based on geometrical features (e.g., moment invariants, principal moments, curve skeletons). The approach is based on a strict isomorphic graph matching, which, however, is considered inadequate for general purpose search systems. Sundar *et al.* [8] proposed a skeleton-based approach where the topological information is obtained from the skeletal graphs and primitive geometrical information is assigned to the graph nodes. The curve skeletons proposed in [9] are utilized for shape matching of 3-D objects in [25], where a many-to-many matching method based on the Earth Mover's Distance is introduced.

In [38], a method which presents some similarities with the proposed approach has been presented. The 3-D object is segmented based on a medial surface segmentation approach and described in terms of a direct acyclic graph of the connected components. The volume ratio of every part is assigned to respective graph node as a geometrical feature. The graphs are indexed and stored in a database. The matching is based on the graph spectra.

The complex representation of skeletal graphs used in the aforementioned methods cannot assign substantial geometric information to the graph elements. In most cases, a perceptually meaningful part of the object, that could enclose adequate geometrical information, is associated with more than one connected graph elements. Thus, the geometrical information associated to the graph is rather trivial. In addition, a more efficient geometric feature should be assigned to each part, which would provide intuitive shape information of the part, retaining at the same time the compactness a skeletal graph structure demands.

3) *Partial Matching Approaches*: Recently, several researchers have investigated approaches for partial shape matching based on feature correspondences. The general idea behind the presented methods is to compute local geometrical descriptors for every object. Then, a cost function is utilized to define the optimal matches, by minimizing the distances between corresponding local features.

In [36], 2-D image registration approaches are extended for 3-D object partial matching applications. For every object, a set of salient points is selected and local shape descriptors

are computed. The matching process utilizes the nonrigid thin-plate-spline (TPS) registration to identify potentially homologous subparts as sets of matching salient point pairs. In [37], a partial matching approach based on salient geometric features is presented. A small number of salient geometric features are extracted and stored using the geometric hashing approach.

In [35], partial matching is performed using the priority-driven search approach. Every object is described by a set of local 3-D geometrical features and the matching attempts to relate any subset of the query's local features with any subset of any object in the database. The process is repeated until all desired matches have been found.

For the majority of the partial matching approaches presented so far, unlike the graph based methods, the resulting correspondences are completely independent of the object topology, thus it is not guaranteed that the retrieved results will be always similar to the query.

4) *The Proposed Approach*: Summarizing, the contribution of this paper is twofold. Firstly, the proposed method can be efficiently used for both partial and global 3-D object search and retrieval. Secondly, a novel combination based on the topological features and the highly discriminative geometrical features of the 3-D object is introduced in order to achieve the latter. The majority of the relevant methods presented so far were focusing either on the geometry, or on the topology of the object. Some recent approaches attempted to combine the geometry with topology, however some major issues have not been addressed so far: The combined approaches are based on segmentation process without taking care of the segmentation result. This can lead to oversegmentation, and thus it is not possible to assign substantial geometric information to the graph elements. In the proposed approach, is attempted to manage the problem by proposing a set of novel rules to avoid oversegmentation. In addition, the combined approaches presented so far use primitive geometrical features (e.g., volume ratios [38], barycentric position of the parts etc). In this approach high discriminative feature vectors are assigned to every graph node in order to achieve better retrieval results. Finally, the proposed approach is capable of performing both global and partial matching using the same graph structure.

More specifically, the topology of a 3-D object is taken into account by extending a 3-D segmentation method based on the medial surface [33] in the sense of creating "meaningful" segments. In general, a meaningful segment represents a component that can be perceptually distinguished from the remaining object [17]. Using the segments' connectivity a graph is formed, where every graph node is associated with an object's segment. The geometry of the object is then taken into account by introducing a novel highly discriminative method for geometric feature extraction: Firstly, every segment of the object is approximated with a superellipsoid and then the novel distance field descriptor (DFD), is computed for each part. The DFD is proven to be invariant to translation, rotation and scaling of the object. Translation and scaling invariance are ensured by the superellipsoid approximation. Rotation invariance is achieved by the superellipsoid approximation combined with the orientation invariant property of the DFD.

Following the aforementioned procedure, an attributed graph is constructed, where each node is attributed with the corresponding DFDs and the parameters of the approximated superellipsoid. For similarity detection, an attributed graph-matching algorithm is then used, which performs both partial and overall matching at once.

The paper is organized as follows. In Section II, the object segmentation method is presented while the graph construction method is analyzed in Section III. In Section IV, the superquadric approximation method is presented and in Section V, the new descriptor is introduced. The matching algorithm is presented in Section VI and the experimental results in Section VII. Finally, conclusions are drawn in Section VIII.

II. SEGMENTATION INTO MEANINGFUL PARTS

In this section, a procedure for efficient extraction of *meaningful segments* from 3-D objects is described. In order to perform the object segmentation, the medial surface-based segmentation method of [33] is extended as follows: Firstly, the medial surface of the object is extracted [29] and segmented [33]. Then, a segment-readjustment technique is proposed in this paper, in order to remove noisy surface parts. This procedure results in a more meaningful medial surface segmentation. Finally, a statistical-based approach is also proposed so as to segment the 3-D object, by assigning every boundary voxel to a medial surface segment.

A. Medial Surface Extraction

The medial surface of an object is the 3-D extension of the medial axis transform (MAT) of an image [30]. MAT has been introduced for biomedical applications [34] and has been used for many 2-D and 3-D applications. Despite its popularity, the numerical computation needed remains non-trivial. Also, many algorithms are very sensitive to surface noise. The method implemented in this paper, is the medial surface extraction proposed in [29] which is fast and robust to surface noise. It is applicable for objects represented in terms of volumetric functions, thus, all the objects represented in other forms (e.g., 3-D meshes) are firstly converted into volumetric functions according to the following process:

Suppose that M is the polygon mesh of a 3-D object. Let $N \times N \times N$ be the size of the smallest cube bounding the mesh. The bounding cube is partitioned in R^3 equal cube shaped voxels u_i with centers \mathbf{v}_i . The size of each voxel is $(N/R)^3$. Let also U be the set of all voxels inside the bounding cube and $U_M \subseteq U$ be the set of all voxels belonging to the bounding cube and lying inside M . Then, the discrete binary volume function $\hat{f}(\mathbf{v})$ of M , is defined as [6]

$$\hat{f}(\mathbf{v}) = \begin{cases} 1, & \text{when } \mathbf{v} \in U_M, \\ 0, & \text{otherwise.} \end{cases}$$

In general, 3-D models have various levels-of-detail, depending on their mesh representation, ranging from a very few to thousands of vertices and triangles. The number R^3 of voxels is kept constant for all models in order to achieve robustness with respect to the level-of-detail [28].

The medial surface extraction algorithm utilized in this paper, based on Hamilton-Jacobi equations, is presented in [29]. The

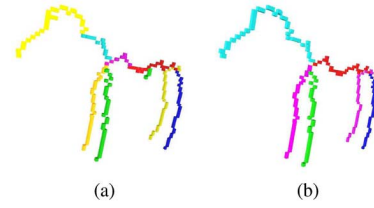


Fig. 1. Medial surface parts (a) before the readjustment step and (b) after the readjustment step.

algorithm is taking advantage of the Hamilton's canonical equations to perform a topological thinning. To achieve the latter, the average outward flux (AOF) of the Euclidean Distance Transform's gradient field (∇D) is computed on every voxel. For the discrete case, the AOF of the voxel \mathbf{x} is defined as

$$\text{AOF}(\mathbf{x}) = \frac{1}{n} \sum_{i=1}^n \langle \nabla D(\mathbf{x}_i), \mathbf{n}_i \rangle \quad (1)$$

where n is the number of neighboring voxels, $\mathbf{x}_i, i = 1 \dots n$ are the neighboring voxels, and \mathbf{n}_i is the outward normal from the voxel \mathbf{x} to the voxel \mathbf{x}_i .

The value of AOF is approaching a negative value around the medial surface points and is close to zero elsewhere. Thus, an appropriate thinning topology preserving approach follows in order to extract the medial surface, so as to take into account the values of the AOF on every voxel. During the topology preserving thinning process, all the voxels from the surface of the object that do not affect the topology of the object and have appropriate AOF value are recursively removed. When none of the voxels can be removed, the remaining shape is the medial surface of the initial object.

B. Medial Surface Segmentation and Segments Readjustment

In order to perform an initial segmentation of the medial surface, every voxel of the medial surface is classified into one of the following categories [33]:

- Simple, when the voxel is an end point of a line, or surface segment or junction.
- Line Voxel, when the voxel belongs to a line segment, but it is not an end point or junction.
- Surface Voxel, when the voxel belongs to a surface segment, but it is not an end point or junction.
- Junction, when the voxel is a junction between two lines, or two segments, or a line and a segment.

The classification process is based on the connectivity of the neighboring medial surface and background voxels as it is presented in [33]. Then, the medial surface is firstly segmented on parts according to the following rules:

- All the neighboring line voxels along with the neighboring simple voxels form a line segment.
- All the neighboring surface voxels along with the neighboring simple voxels form a surface segment [Fig. 1(a)].

Then, the medial surface segments are readjusted in a way that the resulting segments correspond to larger but more meaningful parts of the 3-D object. This is achieved by introducing a

set of simple but effective novel criteria, which can be summarized as follows:

- *The Elimination Criterion:* Segments whose size is considerably small, when compared with the overall medial surface size, are eliminated.
- *The Merging Criterion:* All the adjacent line segments that are connected with *degree* – 2 nodes are merged into one segment. The degree of a node is the number of edges incident to that node. The Merging and Elimination Criterion result in the elimination of several noisy parts, while the general topology remains the same.
- *The Correction Criterion:* This criterion determines a combined elimination-merging action in order to correct specific parts of the new medial surface. According to the Correction Criterion, a segment which lies between two branch nodes and its size is considerably small, when compared to the overall size, is eliminated and the two branch nodes are merged into one.
- *The Oversegmentation Criterion:* This criterion determines if the object has been oversegmented. If the number of resulted parts is comparable to the number of medial surface voxels, then all the parts are merged in one part. In case of one segment, the method simply does not use the topological information and only the geometry is taken into account.

An example of applying the above criteria is given in Fig. 1(b). The medial surface is now segmented into more meaningful parts, when compared to that in Fig. 1(a), while its topology is preserved.

C. Meaningful Parts Assignment Criterion

After readjusting the medial surface segments, a novel method for object decomposition is proposed, where each voxel of the object's boundary surface is assigned to a segment.

In order to determine the assignment criterion, the following definitions are necessary:

- $S = \{\bigcup_{i=1}^n S_i\}$ is the set of medial surface segments and n is the number of medial surface segments.
- $S_i = \{\mathbf{x}_i[k] \mid k = 1 \cdots N_i\}$ is the set of medial surface voxels that belong to segment S_i and $\mathbf{x}_i[k]$ are the coordinates of the k medial surface voxel's center assigned to the i part. N_i is the number of the medial surface voxels assigned to the i segment.
- $P = \{\mathbf{p}[l] \mid l = 1 \cdots L\}$ is the set of boundary voxels; $\mathbf{p}[l]$ are the coordinates of the l boundary voxel's center, $P \subset U_A$, while U_A is the set of voxels lying inside the object A and L is the number of object's boundary voxels.
- $d(\mathbf{p}[l], \mathbf{x}_i[k])$ is the Euclidean distance of the l th boundary voxel from the k th medial surface voxel of the segment S_i .
- $D_i[l] = \arg \min_{1 \leq k \leq N_i} \{d(\mathbf{p}[l], \mathbf{x}_i[k])\}$ is the minimum Euclidean distance of the l th boundary voxel from the segment S_i .
- $P_i = \{\mathbf{p}_i[l] \mid l = 1 \cdots L_i\}$ is a subset of P , which represents the set of boundary voxels assigned to segment S_i and $\mathbf{p}_i[l]$ are the coordinates of the l boundary voxel's center assigned to i part. L_i is the number of boundary voxels assigned to the i part.

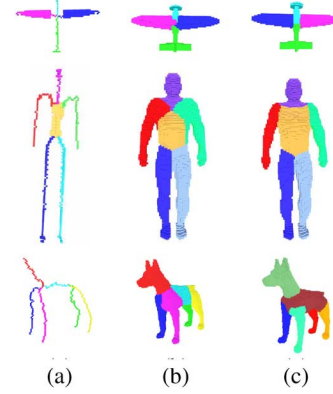


Fig. 2. Segmentation.

A boundary voxel $\mathbf{p}[l]$ is assigned to the segment S_i , i.e., it belongs to P_i , if the following criterion is satisfied:

$$\mathbf{p}[l] \in P_i \Leftrightarrow D_i[l] = \arg \min_{1 \leq i \leq n} \{D_i[l]\} \quad (2)$$

which means that the voxel is assigned to the closest segment S_i , in terms of Euclidean distance. However, this simplified approach may lead to unacceptable results as shown in Fig. 2(b). By examining the margins of the object's segments it is obvious that a meaningful segmentation is not fully achieved. Therefore, a correction step, based on statistical information, is added so as the resulted segmentation is more reasonable.

Let σ_i be the standard deviation of $D_i[l]$ for all boundary voxels $\mathbf{p}_i[l]$ assigned to the segment S_i . The assignment criterion is now modified as

$$\mathbf{p}[l] \in P_i \Leftrightarrow w_i \cdot D_i[l] = \arg \min_{1 \leq i \leq n} \{w_i \cdot D_i[l]\} \quad (3)$$

where w_i is a weight factor given by the following equation:

$$w_i = 1 + \frac{\sigma_i - \arg \min_{1 \leq i \leq n} \sigma_i}{\arg \max_{1 \leq i \leq n} \sigma_i - \arg \min_{1 \leq i \leq n} \sigma_i} \quad (4)$$

and λ an appropriately selected factor. In most cases, this additional correction step improves the segmentation accuracy, as shown in Fig. 2(c). The correction step is based on the assumption that the surface of a segment is uniformly distributed around the medial surface. Some examples of the segmentation process, following the criteria introduced in this paper, are depicted in Fig. 2. More specifically, in Fig. 2(a) is depicted the initial medial surface of a 3-D object, while in Fig. 2(b) the resulting segmentation when the simple criterion of (2) is utilized. In 2(c) the segmentation that results with the usage of the more sophisticated criterion of (3) is shown. From these results it is clear that the final segmentation of the 3-D object is desirable since it is segmented into "meaningful" parts.

D. Benefits of Using 3-D Medial Surface

The usage of medial surface instead of medial axis for segmenting a 3-D object has many advantages since the medial surface encloses more information about the object instead of medial axis in sense that:

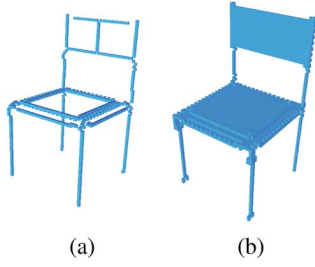


Fig. 3. Differences between (a) medial axis and (b) medial surface.

- medial axis based segmentation fails on segmenting 3-D objects which contain large flat areas (e.g., tables, chairs) due to ambiguity of medial axis for this kind of 3-D objects [Fig. 3(a)]. In contrast, the medial surface is a well-defined transform for all 3-D objects [Fig. 3(b)];
- boundary voxels are more uniformly distributed along the medial surface than the medial axis; as a result, the correction step of the medial surface segmentation algorithm produces more stable results.

III. FROM MEDIAL SURFACE TO GRAPH

The idea introduced in this paper is that an efficient similarity measure for 3-D shape matching should equally rely on high geometrical and topological information. The topological information is maintained in the simple medial surface representation, which has been obtained during the medial surface extraction and readjustment procedures. The high geometrical information is enclosed in the 3-D object's meaningful parts which are assigned to each medial surface segment. This combined information could be uniquely exploited through an appropriate attributed graph-matching technique. Therefore, a transformation from the medial surface representation to an attributed graph is needed.

In a formal way, the graph can be generally represented as $G = \{V, E, \{\mathbf{A}_i\}_{i=1}^r, \{\mathbf{B}_i\}_{i=1}^s\}$ where V is the non-empty set of vertices, E is the set of edges, \mathbf{A}_i is the adjacency matrix based on the i edge attribute, \mathbf{B}_i is the weight vector containing the i weight of all vertices, r is the number of edge attributes and s is the number of vertex attributes.[21] In this work, the edges are undirected and not attributed, thus the graph can be described as $G = \{V, E, \mathbf{A}, \{\mathbf{B}_i\}_{i=1}^s\}$, where \mathbf{A} is a binary symmetric adjacency matrix (if the edges are not attributed, it is assumed that all edges are single attributed with the same value).

The adjacency matrix \mathbf{A} of the graph is constructed as follows.

- The matrix $\mathbf{A} = [a_{jk}]$ is a square $n \times n$ matrix, where $n = |V|$ is the number of segments.
- If the vertices $v_k, v_j \in V$ are connected with the edge e_l and the direction of the edge is from v_k to v_j , then the element a_{kj} of \mathbf{A} is equal to 1. If the edge is undirected, then $a_{jk} = a_{kj}$.
- If the vertices $v_k, v_j \in V$ are not connected, then the element a_{jk} of \mathbf{A} is set to zero.

Based on the above description, the medial surface can be converted to an undirected vertex-attributed graph, according to the following mapping definitions.

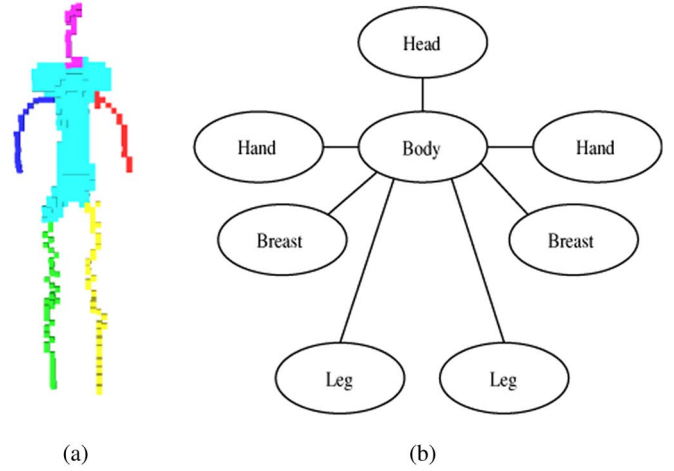


Fig. 4. Transforming (a) medial surface to (b) graph.

- The segments S_i will constitute the vertices v_i of the graph, while their connections the edges e_l . The edges are undirected.
- The attributes of each graph vertex v_i will be obtained from part P_i associated with segment S_i , using the geometrical descriptors extracted for every meaningful part.

Fig. 4 depicts the resulting graph.

IV. SUPERELLIPSOIDS APPROXIMATION

Every extracted segment of the 3-D object P_i is approximated by an appropriate superquadric. Superquadrics have been used in the past to model objects using as input, range images and depth maps [26]. In general, superquadrics is a family of analytical surfaces consisting of superellipsoids, superparaboloids, superhyperboloids, supertoroids, etc. In order to approximate the shape of a 3-D object, surfaces like superellipsoids, which are defined by the implicit (5), are of practical interest:

$$\begin{aligned}
 F(x, y, z) &= \left(\left(\left(\frac{x}{a_1} \right)^{\frac{2}{\varepsilon_2}} + \left(\frac{y}{a_2} \right)^{\frac{2}{\varepsilon_2}} \right)^{\frac{\varepsilon_1}{\varepsilon_2}} + \left(\frac{z}{a_3} \right)^{\frac{2}{\varepsilon_1}} \right)^{\varepsilon_1} \\
 &= 1.
 \end{aligned} \tag{5}$$

In this paper, the superellipsoids have been selected as the most appropriate for describing every segment, because the segments of the objects are expected to have a shape that can be approximated with a superellipsoid, without losing significant shape information.

Function (5) is commonly called inside-outside function, because for a 3-D point with coordinates (x, y, z) :

$$\begin{cases} F(x, y, z) > 1, & \text{if } (x, y, z) \text{ lies outside} \\ & \text{the surface of the object.} \\ F(x, y, z) \leq 1, & \text{if } (x, y, z) \text{ lies inside or on} \\ & \text{the surface of the object.} \end{cases} \tag{6}$$

After the selection of the appropriate superquadric equation to model the 3-D data, the problem of modeling the 3-D object

using a superquadric is reduced to the least squares minimization of the nonlinear inside-outside function $F(x, y, z)$ with respect to several shape parameters. In particular

$$\begin{aligned} F(x, y, z) \\ = F(x, y, z; a_1, a_2, a_3, \varepsilon_1, \varepsilon_2, \phi, \theta, \chi, t_x, t_y, t_z) \end{aligned} \quad (7)$$

where (x, y, z) are the coordinates of a point in the 3-D space, $a_1, a_2, a_3, \varepsilon_1, \varepsilon_2$ are the superquadric shape parameters, ϕ, θ, χ and t_x, t_y, t_z are the Euler angles and translation vector coefficients, respectively. The above parameters are determined so as to minimize the following mean-square error (mse):

$$\text{mse} = \sum_{i=1}^N \sqrt{a_1 a_2 a_3} (F(x_i, y_i, z_i) - 1)^2 \quad (8)$$

where N is the number of points of the 3-D object.

The 3-D object approximation using superquadrics fits well with the method presented in this paper. More specifically, after the 3-D object medial surface extraction and segmentation steps (Section II), each of the extracted meaningful parts P_i can be approximated with an appropriate superellipsoid. The superellipsoid has been chosen as the best, among the family of superquadrics, in terms of approximation effectiveness.

The well-known Levenberg–Marquardt method [26] for nonlinear least squares minimization has been utilized in order to evaluate the shape parameters. The main problem of this minimization method is the need for appropriate initial values. Initial values for shape parameters a_1, a_2, a_3 , translation parameters t_x, t_y, t_z and rotation parameters ϕ, θ, χ are evaluated from the segment size, from the mass center of the segment and from the eigenvectors of segment's inertia matrix. However, there is no safe way to initiate the parameters $\varepsilon_1, \varepsilon_2$ as specific information about the shape is not known in advance. Thus, a brute-force search over an appropriate discrete partition of the domain of $\varepsilon_1, \varepsilon_2$ is utilized in order to specify a global minimum. Finally, the parameters $a_1, a_2, a_3, t_x, t_y, t_z, \phi, \theta, \chi$ and $\varepsilon_1, \varepsilon_2$ of the super-ellipsoid which approximates the part P_i are estimated. From the above set of parameters, the a_1, a_2, a_3 and $\varepsilon_1, \varepsilon_2$ are chosen for the 3-D meaningful part approximation, since they enclose shape information, and will be inserted as attributes to the graph node v_i . Thus, every graph node v_i has been attributed with

$$\mathbf{Z}_{v_i} = [\alpha_1 \ \alpha_2 \ \alpha_3 \ \varepsilon_1 \ \varepsilon_2]^T. \quad (9)$$

An example of super-ellipsoid approximation is given in Fig. 5.

V. 3-D DISTANCE FIELDS DESCRIPTOR

In this section, a novel 3-D descriptor is introduced. Suppose that M is a 3-D object, and $F(a, b, c) = 0$ is the equation that defines an ellipsoid. Then, a descriptor that gives a measure of the difference between the surface of an ellipsoid and the surface of the object can be defined. This is the 3-D DFD. The DFD

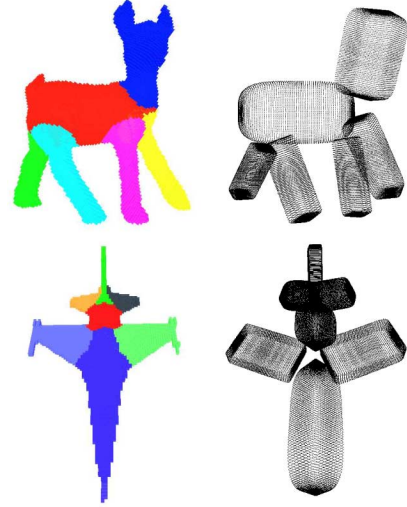


Fig. 5. Super-ellipsoid approximation.

is extra information on the parameters estimated with superellipsoid approximation in order to capture differences between surfaces of segments with similar superellipsoid parameters.

The function that describes the ellipsoid is

$$F(a, b, c) = \frac{x^2}{a^2} + \frac{y^2}{b^2} + \frac{z^2}{c^2} = 0. \quad (10)$$

The object is positioned in the center of the coordinate system and the ellipsoid is sampled uniformly in θ, ϕ of spherical coordinates. For every sample (θ_i, ϕ_j) the signed distance d_{ij} between the surface of the ellipsoid and the surface of the object at the same (θ_i, ϕ_j) is computed and a matrix \mathbf{DF} is formed

$$\mathbf{DF} = [d_{ij}]. \quad (11)$$

It is assumed that the distance is negative if the surface point does not lie on the ellipsoid's interior. Finally, the two dimensional Fourier transform of the \mathbf{DF} matrix is computed and the absolute values of the first μ harmonics (which, in general, are complex numbers) constitute the new 3-D DFD vector $\mathbf{d}_{\mathbf{DF}}$.

$$\mathbf{F}_{\mathbf{DF}} = \mathcal{FT}\{\mathbf{DF}\} \quad (12)$$

$$\mathbf{d}_{\mathbf{DF}} = [\|F_{\mathbf{DF}}(0,0)\| \ \|F_{\mathbf{DF}}(0,1)\| \ \|F_{\mathbf{DF}}(1,0)\| \\ \|F_{\mathbf{DF}}(0,2)\| \ \|F_{\mathbf{DF}}(1,1)\| \ \|F_{\mathbf{DF}}(0,2)\| \ \dots] \quad (13)$$

The 3-D DFD is extracted for every segment of the 3-D object and is followed by a scaling procedure:

$$\mathbf{d}_{\mathbf{DF}}^s = \frac{1}{\sum_i |d_{\mathbf{DF}}(i)|} \mathbf{d}_{\mathbf{DF}}. \quad (14)$$

The scaled 3-D DFD of every part enhances the attributes of the associated graph node. It should be mentioned that there is no need for further scale, rotation and translation normalization, because these parameters have already been computed during the superellipsoid approximation procedure.

The advantages of using the Fourier transform are:

- it is a compact transform, thus the object can be described with a small number of descriptors;

- the Euclidean norm of complex Fourier coefficients is invariant under 90 degrees rotation around axis x, y or z .

Theorem 1: The Euclidean norm of complex Fourier coefficients of a distance field is invariant under 90 degrees rotation around axis x, y or z .

Proof: Suppose that the matrix \mathbf{DF} consists of the signed distances between the object's surface and ellipsoid's surface at the same (θ_i, ϕ_i) . The space of the spherical coordinates $[0, 2\pi) \times [0, \pi]$ is uniformly sampled in a way that:

- if θ_i is a sample, then the $\pi - \theta_i, \pi + \theta_i, (\pi/2) - \theta_i, (\pi/2) + \theta_i$ and $2\pi - \theta_i$ must also be samples;
- if ϕ_i is a sample, then the $\pi - \phi_i, (\pi/2) - \phi_i$ and $(\pi/2) + \phi_i$ must also be samples.

Suppose that $F_{\mathbf{DF}}(\omega_1, \omega_2)$ are the discrete Fourier transform coefficients of the $M \times N$ matrix \mathbf{DF} . Then, from the Fourier transform definition

$$F_{\mathbf{DF}}(\omega_1, \omega_2) = \sum_{m=0}^{M-1} \sum_{n=0}^{N-1} \mathbf{DF}(m, n) e^{-j\frac{2\pi m\omega_1}{M}} e^{-j\frac{2\pi n\omega_2}{N}} \quad (15)$$

Suppose that the object is rotated 90 degrees around the z axis. Then, the new distance field matrix is:

$$\mathbf{DF}'(m, n) = \mathbf{DF} \left(\left(m + \frac{M}{4} \right) \bmod M, n \right) \quad (16)$$

which is a translated version of the initial matrix.

The Fourier coefficients are computed as in (17)

$$\begin{aligned} F'_{\mathbf{DF}}(\omega_1, \omega_2) &= \sum_{m=0}^{M-1} \sum_{n=0}^{N-1} \mathbf{DF}'(m, n) e^{-j\frac{2\pi m\omega_1}{M}} e^{-j\frac{2\pi n\omega_2}{N}} \\ &= \sum_{m=0}^{M-1} \sum_{n=0}^{N-1} \mathbf{DF} \left(\left(m + \frac{M}{4} \right) \bmod M, n \right) \\ &\quad \times e^{-j\frac{2\pi m\omega_1}{M}} e^{-j\frac{2\pi n\omega_2}{N}} \\ &= \sum_{m=0}^{M-1} \sum_{n=0}^{N-1} \mathbf{DF} \left(\left(m + \frac{M}{4} \right) \bmod M, n \right) \\ &\quad \times e^{-j\frac{2\pi(m+M/4)\omega_1}{M}} e^{-j\frac{2\pi n\omega_2}{N}} e^{j\frac{2\pi M/4\omega_1}{M}} \\ &= F_{\mathbf{DF}}(\omega_1, \omega_2) e^{j\frac{\pi\omega_1}{2}} \end{aligned} \quad (17)$$

leading in

$$\|F_{\mathbf{DF}}(\omega_1, \omega_2)\| = \|F'_{\mathbf{DF}}(\omega_1, \omega_2)\|. \quad (18)$$

In a similar manner, the theorem can be extended for degree rotations around axis x and y . The extension of the above theorem for any $k(\pi/2), k \in \mathbb{N}$ rotation around the z axis is trivial.

Theorem 2: The 3-D DFD of a rotation normalized object is rotation invariant.

Proof: Suppose that the object M is rotation normalized, either using PCA, or using the parameters estimated during the superellipsoid approximation process. However, there is no knowledge concerning the orientation of the three principal axis, thus there is an ambiguity of 180° rotation around x, y

or z axis. Suppose that the 3-D DFD of the M is extracted. Then, according to Theorem 1, the ambiguity is dropped and the extracted descriptor is fully rotation invariant.

In this paper, during the superellipsoid approximation procedure, the estimated rotation parameters ϕ, θ, χ define an orthogonal coordinate system with ambiguity on the direction of every axis, due to the symmetry of the superellipsoid.

VI. MATCHING

The graph, produced from the 3-D object, along with the super-ellipsoid parameters assigned to each node, form a vertex attributed graph. In order to align two graphs for matching purposes, an attributed graph-matching technique is applied.

To calculate the similarity between two objects A and B described with the undirected vertex-attributed graphs $G_A = \{V_A, E_A, \{\mathbf{A}^A\}, \{\mathbf{B}_i^A\}_{i=1}^s\}$, $|V_A| = n_A$ and $G_B = \{V_B, E_B, \{\mathbf{A}^B\}, \{\mathbf{B}_i^B\}_{i=1}^s\}$, $|V_B| = n_B$, respectively, the two graphs are aligned based on the successive projection graph-matching algorithm (SPGM), proposed by B.J. van Wyk [21], [22]. By utilizing this algorithm, a matrix $\tilde{\mathbf{P}}$ is computed, which is a constrained estimation of the permutation matrix \mathbf{P} , which transforms G_A to G_B .

According to the SPGM algorithm, the problem of attributed graph matching is transformed to an optimization problem. More specific, the matrix $\tilde{\mathbf{P}}$ is computed by minimizing the following function:

$$J(\mathbf{p}) = -\frac{1}{2}\mathbf{p}^T \mathbf{X} \mathbf{p} - \frac{1}{2}\mathbf{p}^T \mathbf{I} \mathbf{p} - \mathbf{y}^T \mathbf{p} \quad (19)$$

where $\mathbf{p} = \text{vec}(\tilde{\mathbf{P}})$ ($\text{vec}(\cdot)$ denotes the vectorization operation). \mathbf{X} is a matrix of compatibility values between edges, \mathbf{y} is a vector of compatibility values between vertices, and \mathbf{I} is the appropriate identity matrix. The elements of the matrix \mathbf{X} are computed using (20) and the elements of the vector \mathbf{y} are computed using (21)

$$X_{kl} = \frac{\alpha}{\sum_{g=1}^r \left| A_{l-\lfloor \frac{l-1}{n} \rfloor n, k-\lfloor \frac{k-1}{n} \rfloor n}^g - A_{1+\lfloor \frac{l-1}{n} \rfloor, 1+\lfloor \frac{k-1}{n} \rfloor}^g \right| + \alpha} \quad (20)$$

$$y_k = \frac{\alpha}{\sum_{h=1}^s \left| B_{k-\lfloor \frac{k-1}{n} \rfloor n}^h - B_{1+\lfloor \frac{k-1}{n} \rfloor}^h \right| + \alpha}. \quad (21)$$

The required constraints are

$$\text{Constraints: } \begin{cases} 0 \leq \tilde{P}_{ij} \leq 1 \\ \sum_{i=0}^{n_A} \tilde{P}_{ij} \leq 1 \forall j \\ \sum_{j=0}^{n_B} \tilde{P}_{ij} = 1 \forall i \end{cases} \quad (22)$$

The matching process is performed in pairs, in a two-step procedure. Suppose that the objects A and B are described with the undirected edge-attributed graphs G_A and G_B . The SPGM algorithm is applied on the graphs G_A and G_B , assuming that the graphs are attributed only with the superellipsoid parameters. The result is a probability matrix $\tilde{\mathbf{P}} = [p_{ij}]$. Every element p_{ij} expresses the probability that the i segment of the first object matches with the j segment of the second object. If a pair of segments (sub-objects) is probably matched, then a dissimilarity

metric can be computed, exploiting the 3-D DFD, the superellipsoid approximation and the Mahalanobis L_1 norm

$$D_{ij} = \frac{w_{sq}}{S} \sum_{r=1}^3 |a_{r_i} - a_{r_j}| + w_{DF} \sum_{r=1}^F |F_{DF_i}(r) - F_{DF_j}(r)| \quad (23)$$

where S is a constant scaling factor proportional to the voxel model size and F is the number of the DFD's harmonics used to describe each part.

To determine the most probable matches, the probability matrix \bar{P} is considered according to the following novel criteria proposed in this paper.

- If $p_{ij} > p_{thres}$, then the pair is marked as High Probability Pair
- Otherwise, the probabilities p_{ix}, p_{yj} are considered, where $x \in [1, \dots, n_A]$ and $y \in [1, \dots, n_B]$, as follows:
 - If $(|p_{ij} - p_{ix}|/p_{ij}) > \text{Threshold}$ then the (i, x) pair is marked as Possible.
 - The same procedure is followed for the probabilities p_{xj} .
 - The dissimilarity metric for every pair marked as Possible is computed and the pair having the minimum dissimilarity metric is selected.
 - If the dissimilarity metric is below a threshold, then the selected pair is marked as a High Probability Pair. Otherwise, it is marked as a Low Probability pair.

The global metric is then computed using the equation

$$D(A, B) = \frac{1}{N_{pairs}} \sum_{r=1}^{N_{pairs}} W_r D(\text{pair}(r)) \quad (24)$$

where W_r is a weight factor per segment pair proportional to segment size and N_{pairs} is the number of matched pairs of segments. The W_r has been selected to be proportional to the segment volume in order to avoid matching of less significant parts, assuming that the parts with bigger volumes are more significant.

For the partial matching application only the high probability pairs are considered, while for the global matching application, both high and low probability pairs are used. Moreover, for global matching application, p_{thres} is less strict.

VII. EXPERIMENTAL RESULTS

The proposed method was evaluated using the Princeton Shape Benchmark (PSB)[27] consisting of 1814 objects, as dataset and as queries the 30 objects provided by the SHape REtrieval Contest 2006 (SHREC 2006) [40]. The dataset was enhanced with objects having missing parts for the needs of the partial matching evaluation.

The database consists of 3-D models in OFF format. A pre-processing step for converting the mesh representation into a volumetric representation was needed in order to compute the curve skeletons for each model. The 3-D mesh [Fig. 6(a)] is enclosed in the smallest bounding cube which is then partitioned

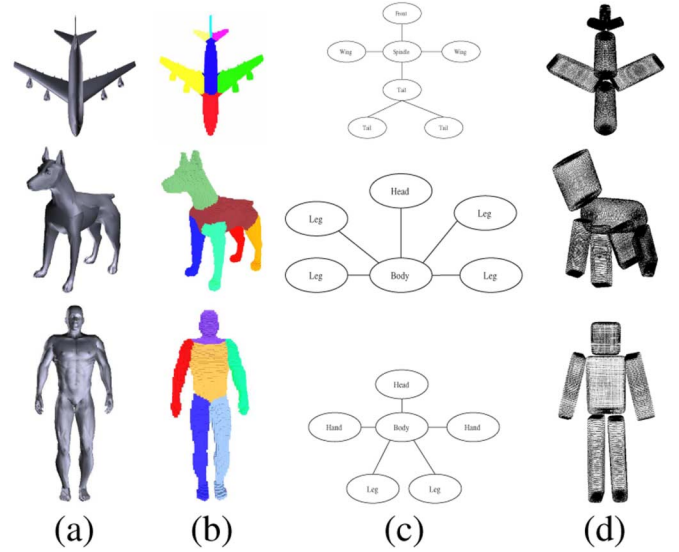


Fig. 6. Segmentation results.

in a set of equally cube shaped voxels, using the method presented in [6]. The resolution of the bounding box was selected to be $96 \times 96 \times 96$ voxels. Then, the medial surface is extracted and segmented in order to segment the surface of the 3-D object according to the method presented in Section II [Fig. 6(b)]. From the connectivity of the medial surface segments a graph is constructed [Fig. 6(c)] and attributed with the superellipsoid parameters [Fig. 6(d)] and the 3-D DFD of the associated model segment.

After the segmentation process, a mathematical description of each meaningful part is required so as to efficiently and robustly describe it. The super-quadratics have been chosen because they can produce a very compact representation of the 3-D segments (only five parameters are needed). Further, it is clear that the usage of generic super-quadratics leads in a finer part approximation when compared to the sphere, or the ellipsoid approximation. Moreover, in order to extract a detailed and discriminative descriptor vector for every part, the DFD has been proposed, which is invariant to 90 degrees rotations. The use of a highly discriminative vector increases significantly the retrieval accuracy, especially in the cases where the segmentation fails and results in a one-segment object.

From the Fig. 6, it can be easily observed that the superellipsoid approximation provides an acceptable representation of the object's meaningful parts, while the shape information of each part is significantly reduced to five attributes which are the parameters of the super-ellipsoid.

A. Complexity and Time Issues

In the sequel the complexity issues concerning significant parts of the method are discussed.

- *The Medial Surface Extraction Process:* the complexity of the medial surface extraction algorithm is $O(n \log n)$ [30], where n is the total number of voxels. Thus, for objects with large volume the required time for medial surface extraction is relatively high.

- *The Levenberg–Marquardt Minimization Method*: implemented for the superellipsoid approximation is not complex, as it has been implemented for close to real time collision detection processes [42]. If the brute-force search of two parameters (ε_1 and ε_2) along with the fact that this process is performed for every segment are taken into account, the complexity of approximation is at least $O(mkl)$, where l is the number of segments, k and m are the number of samples in the fields of ε_1 and ε_2 , respectively. However, the total number of segments, using the rules presented in Section II, is kept considerably small. Moreover, the domain of ε_1 and ε_2 is the same ($\varepsilon_1, \varepsilon_2 \in (0, 2)$) and the number of required parts is small.
- *The DFD*: the DFD extraction algorithm complexity is analyzed into two processes: The first one is the field computation with complexity of $O(rt)$ where r and t is the number of samples for the θ and ϕ spherical coordinates. The second process is the Fourier Transform. In order to exploit the properties of Fast Fourier Transform with complexity $O(rt \log r \log t)$, a “smart” sampling of θ and ϕ ($r, t = 2^p$) is performed. As a result, the complexity of DFD for a single part is $O(rt \log r \log t)$.
- *The Attributed Graph Matching*: According to [22] the initial SPGM algorithm has worst-case complexity near $O(n_A^2 n_B^2)$, where n_A, n_B is the number of graph nodes of the two graphs. However, in [21] are also presented methods that reduce the complexity significantly. Moreover, trivial trade-off tricks between processing time and memory could be applied in order to reduce further the complexity. Finally, the resulting graphs are considerably small and equal to the number of object’s segments.

Many precautions have been considered in the proposed algorithm in order to ensure its robustness.

- *Segmentation*: The first aspect is the robustness of the segmentation process. In order to avoid oversegmentation, the novel rules of Section II was proposed and the results prove the robustness and the effectiveness of the segmentation.
- *Superellipsoid Approximation*: Another robustness aspect is identified in the approximation technique implemented in Section IV. It is well-known that for any optimization problem, robustness depends on the initial conditions. For the superellipsoid approximation of every segment, very good initial values can be computed for the majority of parameters (e.g., the initial values for size and rotation parameters can be easily computed by applying Principal Component Analysis). For the shape parameters, $\varepsilon_1, \varepsilon_2$, where no initial estimation could be computed, a robust result can be derived by performing an exhaustive search of their domain.
- *Attributed Graph Matching*: The attributed graph-matching algorithm implemented is referred to be the most robust among a number of similar algorithm presented in [21].

In Table I, the mean times for every part of the proposed approach are given. The times have been measured using an Pentium 3.2-GHz PC with 1-GB RAM running Windows XP.

On average, the time needed for the extraction of the attributed graph for one 3-D model is about 90 s, while the time

TABLE I
AVERAGE TIME FOR EVERY PART OF THE METHOD

Process	Average Time
Voxelization	9.3 sec
Medial Surface Extraction	12.5 sec
Segment Readjustment	1.1 sec
Superellipsoid Approximation (per segment)	4.7 sec
Distance Field Descriptor (per segment)	3.1 sec
Average Processing Time per object	91.5 sec
Matching two 3D objects	0.1 msec

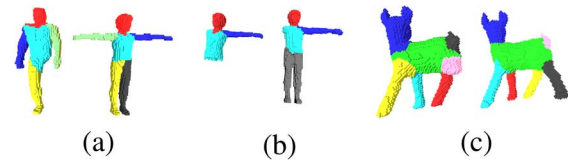


Fig. 7. Performing partial matching.

needed for the comparison of two graphs is about 0.1 ms. It should be clearly stated that the extraction process is performed only once and the resulting graphs can be stored along with the corresponding 3-D models. Since the time needed for the comparison of the feature vectors is very short, the proposed method is very appropriate for use as an efficient tool for web-based, real-time search, and retrieval applications.

B. Partial Matching

Firstly, the proposed framework was tested for its performance in terms of partial matching accuracy.

Fig. 7(a) shows the matching parts indicated with the same colour between a human with a missing leg and a normal human. Fig. 7(b) depicts the matching parts between a human body having only the head and a single arm and a human with a missing arm, while Fig. 7(c) depicts an animal with a missing leg and a normal animal. The matching pairs are painted with the same color, apart from the segments in black, which do not match.

The value of p_{thres} , required for the matching process, was selected to be equal to $(2/3)$. This choice has been motivated by the fact that, for partial matching applications, the best matching parts have to be found, in contrast with global matching applications where a global dissimilarity metric should be computed. Thus, the graph nodes should be matched with higher probability. The weight factors w_{SQ} and w_{DF} have been experimentally selected to be $w_{\text{SQ}} = 0.4$ and $w_{\text{DF}} = 0.6$.

As can be seen from Fig. 7(c), the matching is not absolutely correct, since the legs of the left object do not match with the corresponding legs of the right object. However, this result can be easily explained by examining the connectivity graphs of the objects and the geometrical information of each segment. First

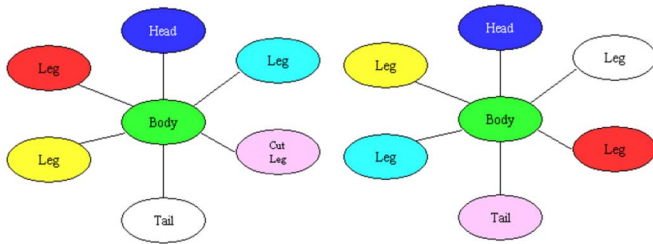


Fig. 8. Graphs of objects of Fig. 7(c).

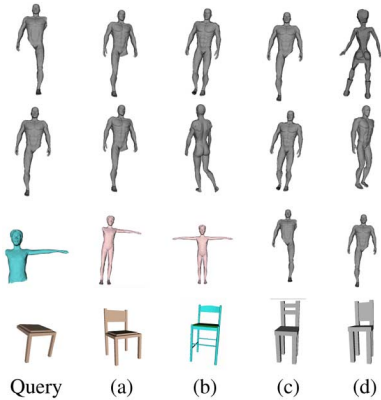


Fig. 9. Example queries, for partial matching.

of all, it is obvious that there is no major geometrical difference between the animal legs. Thus, the variations of the estimated superellipsoid parameters and the computed DFD are small. Furthermore, as it is depicted in Fig. 8, the graphs of the two objects are isomorphic, and the mutual alternation between the legs, does not affect the graph topology.

Fig. 9 depicts the retrieved results for example queries, using the proposed framework for partial matching. The first model is the query model, while the rest are the first four retrieved results. The retrieved results prove the effectiveness of the proposed framework in partial matching applications when the object has missing parts.

C. Global Matching

The effectiveness of the proposed shape-matching method was also evaluated in terms of 3-D object retrieval performance. In this case, each query model of the SHREC 2006 query dataset was used as a query and the retrieved results were ranked in terms of similarity to the query. The similarity matching is based both on topological (medial surface graph correspondence) and geometrical (superellipsoid parameters and 3-D DFD) criteria.

The retrieval performance was evaluated in terms of the following metrics:

- Average dynamic recall (ADR)[39], which measures how many of the documents that should have appeared before or at a given position in the result list actually have appeared.
- First tier (FT) [27], which is the percentage of similar models that appear within the top K matches, where K is the number of similar objects in the dataset.

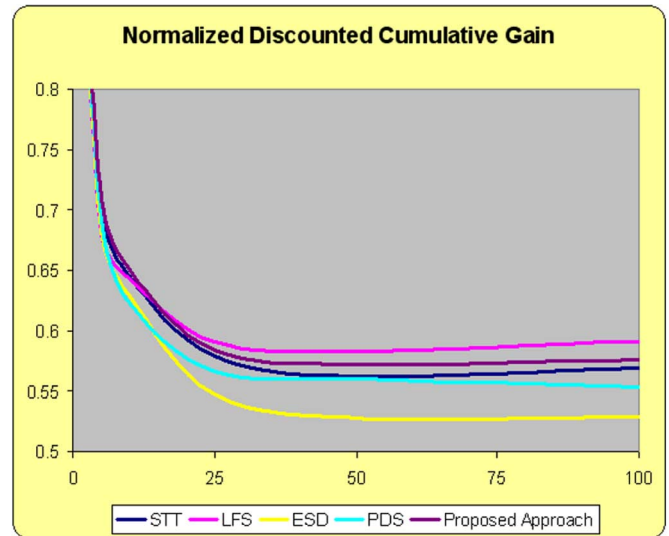


Fig. 10. Normalized cumulative gain diagram comparing the participant methods of SHREC 2006 with the proposed approach.

- Second tier (ST)[27], which is the percentage of similar models that appear within the top K matches, where K is twice the number of similar objects in the dataset.
- Normalized discounted cumulative gain (NDCG) diagram which depicts the effectiveness of the retrieval approach during retrieval [40].

The proposed method was compared to the methods that participated in the SHREC 2006. The participants were:

- priority driven search (PDS) [35] (Run 3);
- a version of the spherical trace transform (STT) [41];
- the light field similarity for model retrieval (LFS) (Run 2);
- the concrete radialized spherical projection descriptor (CRSPD);
- the canonical 3-D Hough transform descriptor (C3DHTD);
- 3-D model retrieval using spherical extent functions and wavelet descriptors (SEFWD) (Run 1);
- enhanced silhouette and depth-buffer based approaches for 3-D shape retrieval (ESD) (Run 1);
- an engineering drawing approach to 3-D shape retrieval (EDA) (Run 2).

The participants could submit up to five different runs, for a different set of parameters. For the needs of this paper, only the best set of parameters, based on ADR has been kept. A brief description of all the above methods can be found in the proceedings of SHREC 2006 [40].

The value of p_{thres} , required for the matching process, was selected to be equal to 0.5. This choice has been motivated by the fact that for global matching approaches, every part of the object should be matched in order to compute a global metric. Thus, the graph nodes should be matched even with lower probability, and the Low Probability pairs are considered during the dissimilarity calculation. The weight factors w_{SQ} and w_{DF} have been experimentally selected to be $w_{SQ} = 0.4$ and $w_{DF} = 0.6$.

Table II presents the comparative results for the Average Dynamic recall, the First-Tier and the Second Tier, while in Fig. 10 depicts the retrieval accuracy of the methods in terms of the Mean NDCG diagram. The results presented below for all

TABLE II
AVERAGE DYNAMIC RECALL, FIRST TIER AND SECOND TIER

Rank	Approach	ADR	Rank	Approach	1st-Tier	Rank	Approach	2nd-Tier
1	LFS	0.549	1	LFS	0.447	1	LFS	0.2786
2	Proposed method	0.525	2	Proposed method	0.428	2	STT	0.2566
3	STT	0.524	3	STT	0.427	3	PDS	0.2563
4	ESD	0.500	4	CRSPD	0.418	4	Proposed method	0.2562
5	CRSPD	0.495	5	PDS	0.409	5	CRSPD	0.2561
6	PDS	0.493	6	C3DHTD	0.392	6	C3DHTD	0.2501
7	C3DHTD	0.492	7	ESD	0.381	7	ESD	0.2285
8	SEFWD	0.306	8	SEFWD	0.241	8	SEFWD	0.1525
9	EDA	0.230	9	EDA	0.172	9	EDA	0.1222

Average Dynamic Recall First Tier Second Tier

TABLE III
AVERAGE DYNAMIC RECALL FOR CHAIR, AIROPLANE, SEDAN, GUN, AND HAND QUERY

	Method	ADR												
1	Proposed method	0.968	1	Proposed method	0.908	1	LFS	0.867	1	CRSPD	0.725	1	Proposed method	0.631
2	LFS	0.959	2	CRSPD	0.847	2	ESD	0.838	2	LFS	0.713	2	STT	0.598
3	C3DHTD	0.912	3	LFS	0.836	3	CRSPD	0.777	3	STT	0.682	3	C3DHTD	0.483
4	PDS	0.824	4	C3DHTD	0.714	4	Proposed method	0.776	4	Proposed method	0.651	4	LFS	0.332
5	STT	0.818	5	SEFWD	0.648	5	STT	0.771	5	ESD	0.646	5	PDS	0.202
6	ESD	0.759	6	STT	0.624	6	C3DHTD	0.717	6	C3DHTD	0.598	6	EDA	0.123
7	CRSPD	0.750	7	ESD	0.567	7	PDS	0.663	7	SEFWD	0.581	7	SEFWD	0.095
8	EDA	0.617	8	EDA	0.563	8	EDA	0.603	8	PDS	0.546	8	ESD	0.043
9	SEFWD	0.369	9	PDS	0.561	9	SEFWD	0.316	9	EDA	0.273	9	CRSPD	0.000

Chair query Airplane query Sedan query Gun query Hand query

methods (except for the results of the proposed method) have been derived from the SHREC 2006 proceedings [40].

It is obvious that for global matching applications, the proposed approach is ranked second. However, the method which was ranked first, utilizes 2-D approaches (as a light-field-based method) and, thus, is not a pure 3-D method. However, outperforms all the pure 3-D based approaches, including the priority-driven search proposed in [35].

In Table III, the proposed approach's average dynamic recall values for specific queries are compared to the other SHREC 2006 participants, while in Fig. 11 the retrieved results for the same queries using the proposed framework, are presented. The first model is the query model, while the rest are the first four retrieved results.

Some interesting result are presented in the last three lines of the retrieved results. When the query is the chair (last line),

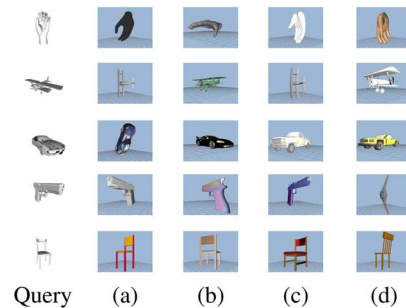


Fig. 11. Retrieved results for global matching.

the proposed approach retrieves chairs, however, some of them could be topologically different. However, their topological similarity is quite enough to discriminate them from the other

classes. It should also be clearly stated that there is no method that perfectly discriminates all the objects of all possible classes and thus, also the proposed method gives some not perfect results. When the query is a car, the segmentation into meaningful parts failed and only geometrical information has been taken into account, based on the oversegmentation criterion presented in Section II. Thus, the results are not the best (although the last two objects are vehicles and belong to the same superclass with the query, they belong to a different subclass). However, the geometric similarity of the results compared to the query is obvious.

From the aforementioned results it becomes clear that the proposed method has excellent performance when the segmentation process is accurate, since in this case we take advantage of very important information contained in the model (both topological and geometrical). This depends mainly on the usage of the medial surface and the segmentation rules which were introduced in this paper and improve significantly this process, and of course on the shape of the 3-D model. In case a 3-D model produces only one segment or a big number of segments, the segmentation process does not take place. Instead, only the super-ellipsoid approximation and the extraction of descriptors based on the distance fields are used.

VIII. CONCLUSION

In this paper, a novel framework for partial and global 3-D shape matching and retrieval was proposed, which relies almost equally on the topology and the geometry of the object. A novel 3-D segmentation algorithm was introduced as an extension of the medial surface segments in order to extract the meaningful object parts. Every part was then approximated with a superellipsoid and the novel 3-D DFD which is invariant under 90 degree rotations around axis x , y and z , was computed. During the matching process, performed in pairs, firstly an attributed graph-matching algorithm was utilized, using as attributes local geometrical features. Finally, a dissimilarity metric, which efficiently combines the results of the graph-matching procedure and the distance between more complex geometrical features is computed.

The framework is suitable for both partial and global matching, as it is figured in the presented experimental results. The main contributions of the proposed framework are:

- a medial surface based segmentation method is introduced, based on the segments of the medial surface;
- a novel compact descriptor, the 3-D DFD, which is invariant under 90 degrees rotation around axis x , y or z , is introduced;
- a main advantage of the proposed framework, derives from the non np -complete graph-matching algorithm utilized, which permits one-to-one association between segments for further matching;
- the proposed framework is among the first ones which performs both partial and global matching at the same time, relying almost equally on both topological and local geometrical features, while the majority of the methods are based only either on geometry or on topology. Furthermore, the

local geometric descriptor can be changed or enhanced by any other global descriptor extraction method, which can be applied separately on every segment.

REFERENCES

- [1] J. W. H. Tangelder and R. Veltkamp, "A survey of content based 3D shape retrieval methods," in *Shape Modeling Applications 2004, Proceedings 7-9*, Jun. 2004.
- [2] N. Iyer, Y. Kalyanaraman, K. Lou, S. Jayanti, and K. Ramani, "A reconfigurable, intelligent 3D engineering shape search system part I: Shape representation," in *Proc. ASME DETC'03, 23rd Computers and Information in Engineering (CIE) Conf.*, Chicago, IL, Sep. 2-6, 2003.
- [3] K. Lou, S. Jayanti, N. Iyer, Y. Kalyanaraman, K. Ramani, and S. Prabhakar, "A reconfigurable, intelligent 3D engineering shape search system part II: Database indexing, retrieval and clustering," in *Proc. ASME DETC' 03, 23rd Computers and Information in Engineering (CIE) Conf.*, Chicago, IL, Sep. 2-6, 2003.
- [4] N. Iyer, K. Lou, S. Jayanti, Y. Kalyanaraman, and K. Ramani, "A multi-scale hierarchical 3D shape representation for similar shape retrieval," in *Proc. TMCE 2004—Tools and Methods for Competitive Engineering*, Lausanne, Switzerland, vol. 2, pp. 1117-1118, TMCE.
- [5] I. Kolonias, D. Tzovaras, S. Malassiotis, and M. G. Strintzis, "Fast content-based search of VRML models based on shape descriptors," *IEEE Trans. Multimedia*, vol. 7, no. 1, pp. 114-126, Feb. 2005.
- [6] P. Daras, D. Zarpalas, D. Tzovaras, and M. G. Strintzis, "Efficient 3D model search and retrieval using generalized radon transforms," *IEEE Trans. Multimedia*, vol. 8, no. 1, pp. 101-114, Feb. 2006.
- [7] A. Kadyrov and M. Petrou, "The trace transform and its applications," *IEEE Trans. Pattern Anal. Mach. Intell.*, vol. 23, no. 8, pp. 811-828, Aug. 2001.
- [8] H. Sundar, D. Silver, N. Gagvani, and S. Dickinson, "Skeleton based shape matching and retrieval," in *Shape Modelling Int.*, 2003, pp. 130-139.
- [9] N. Cornea, D. Silver, X. Yuan, and R. Balasubramanian, "Computing hierarchical curve-skeletons of 3D objects," *Vis. Comput.*, vol. 21, no. 11, pp. 945-955, Oct. 2005.
- [10] D. Y. Chen, X. P. Tian, Y. T. Shen, and M. Ouhyoung, "On visual similarity based 3D model retrieval," *Computer Graphics Forum (EUROGRAPHICS'03)*, vol. 22, no. 3, pp. 223-232, Sep. 2003.
- [11] D. Vranic and D. Saupe, "Description of 3D-shape using a complex function on the sphere," in *Proc. IEEE Int. Conf. Multimedia and Expo*, 2002, pp. 177-180.
- [12] D. V. Vranic, D. Saupe, and J. Richter, "Tools for 3D-object retrieval: Karhunen-Loeve transform and spherical harmonics," in *Proc. IEEE MMSP 2001*, Cannes, France, 2001, pp. 293-298.
- [13] N. Canterakis, "3D Zernike moments and zernike affine invariants for 3D image analysis and recognition," in *Proc. 11th Scandinavian Conf. Image Analysis*, 1999.
- [14] M. Hilaga, Y. Shinagawa, T. Kohmura, and T. L. Kunii, "Topology matching for fully automatic similarity estimation of 3D shapes," in *ACM SIGGRAPH 2001*, Jul. 2001, pp. 203-212.
- [15] D.-Y. Chen and M. Ouhyoung, "A 3D object retrieval system based on multi-resolution reeb graph," in *Proc. Computer Graphics Workshop*, Tainan, Taiwan, R.O.C., Jun. 2002, p. 16.
- [16] T. Tung and F. Schmitt, "Augmented reeb graphs for content-based retrieval of 3D mesh models," in *Proc. Int. Conf. Shape Modeling and Applications 2004 (SMI'04)*, 2004, pp. 157-166.
- [17] S. Katz and A. Tal, "Hierarchical mesh decomposition using fuzzy clustering and cuts," *ACM Trans. Graph.*, pp. 954-961, Jul. 2003.
- [18] M. Kazhdan, T. Funkhouser, and S. Rusinkiewicz, "Rotation invariant spherical harmonic representation of 3D shape descriptors," in *Proc. Eurographics Symp. Geometry Processing*, 2003.
- [19] "MPEG-7 visual part of eXperimentation model (version 9.0)," in *ISO/MPEG N3914, MPEG Pisa Meeting*, Pisa, Italy, 2001, MPEG Video Group.
- [20] M. Novotni and R. Klein, "3D Zernike descriptors for content based shape retrieval," in *Proc. 8th ACM Symp. Solid Modeling and Applications*, Seattle, WA, 2003, pp. 216-225.
- [21] B. J. van Wyk, "Kronecker product, successive projection and related graph matching algorithms," Ph.D. dissertation, Univ. Witwatersrand, Johannesburg, South Africa, May 2003.
- [22] B. J. van Wyk and M. A. van Wyk, "A POCS-based graph matching algorithm," *IEEE Trans. Pattern Anal. Mach. Intell.*, vol. 26, no. 11, pp. 1526-1530, Nov. 2004.

- [23] K. Moustakas, P. Daras, D. Tzovaras, and M. G. Strintzis, "Classification of 3D models using combined semantical and geometrical information," in *Proc. 1st Int. Workshop Towards Semantic Virtual Environments (SVE2005)*, Villars, Switzerland, Mar. 2005.
- [24] N. D. Cornea, D. Silver, and P. Min, "Curve-Skeleton applications," in *Proc. IEEE Visualization 2005-(VIS'05)*, 2005, p. 13.
- [25] N. D. Cornea, M. F. Demirci, D. Silver, A. Shokoufandeh, S. J. Dickinson, and P. B. Kantor, "3D object retrieval using many-to-many matching of curve skeletons," in *Proc. Int. Conf. Shape Modeling and Applications-SMI 2005*, Boston, MA, Jun. 2005.
- [26] F. Solina and R. Bajcsy, "Recovery of parametric models from range images: The case for superquadrics with global deformations," *IEEE Trans. Pattern Anal. Mach. Intell.*, vol. 12, no. 2, pp. 131–147, Feb. 1990.
- [27] P. Shilane, P. Min, M. Kazhdan, and T. Funkhouser, "The Princeton shape benchmark," *Shape Modeling Int.*, pp. 167–178, Jun. 2004.
- [28] D. V. Vranic and D. Sauge, "3D shape descriptor based on 3D fourier transform," in *Proc. EURASIP Conf. Digital Signal Processing for Multimedia Communications and Services (ECMCS2001)*, Budapest, Hungary, Sep. 2001.
- [29] K. Siddiqi, S. Bouix, A. Tannenbaum, and S. W. Zucker, "The Hamilton-Jacobi skeleton," in *Proc. Int. Conf. Computer Vision (ICCV)*, Corfu, Greece, 1999, pp. 828–834.
- [30] K. Siddiqi, S. Bouix, A. Tannenbaum, and S. W. Zucker, "Hamilton-Jacobi Skeletons," *Int. J. Comput. Vis.*, vol. 48, no. 3, pp. 215–231, 2002.
- [31] D. V. Vranic, "3D Model Retrieval," Ph.D. dissertation, Univ. Leipzig, Leipzig, Germany, 2004.
- [32] N. Amenta and R. Kolluri, "The medial axis of a union of balls," *Comput. Geom.: Theory and Applic.*, vol. 20, no. 1–2, pp. 25–37, 2001.
- [33] G. Malandain, G. Bertrand, and N. Ayache, "Topological segmentation of discrete surfaces," *Int. J. Comput. Vis.*, vol. 10, no. 2, pp. 183–197, 1993.
- [34] H. Blum, "Biological shape and visual science," *J. Theoret. Biol.*, vol. 38, pp. 205–287, 1973.
- [35] T. Funkhouser and P. Shilane, "Partial matching of 3D shapes with priority-driven search," in *Euographics Symp. Geometric Processing*, Sardinia, Italy, Jul. 2006.
- [36] M. Novotni, P. Degener, and R. Klein, Correspondence Generation and Matching of 3D Shape Subparts Friedrich-Wilhelms-Univ. Bonn, Bonn, Germany, Tech. Rep. CG-2005-2, Jun. 2005.
- [37] R. Gal and D. Cohen-Or, "Salient geometric features for partial shape matching and similarity," *ACM Trans. Graph.*, vol. 25, no. 1, pp. 130–150, Jan. 2006.
- [38] J. Zhang, K. Siddiqi, D. Macrini, A. Shokoufandeh, and S. Dickinson, "Retrieving articulated 3-D models using medial surfaces and their graph spectra," in *Proc. Int. Workshop Energy Minimization Methods in Computer Vision and Pattern Recognition*, St. Augustine, FL, 2005.
- [39] R. Typke, R. C. Veltkamp, and F. Wiering, "Evaluating retrieval techniques based on partially ordered ground truth lists," in *Proc. Int. Conf. Multimedia and Expo (ICME)*, 2006.
- [40] R. C. Veltkamp, R. Ruijsenaars, M. Spagnuolo, R. van Zwol, and F. ter Haar, SHREC2006, 3D Shape Retrieval Contest Univ. Utrecht, Utrecht, The Netherlands, Tech. Rep. UU-CS-2006-030, 2006 [Online]. Available: <http://www.aimatshape.net/event/SHREC>, URL
- [41] D. Zarpalas, P. Daras, A. Axenopoulos, D. Tzovaras, and M. G. Strintzis, "3D model search and retrieval using the spherical trace transform," *EURASIP J. Adv. Signal Process.*, vol. 2007, no. 23912, p. 14, 2007.
- [42] K. Moustakas, D. Tzovaras, and M. G. Strintzis, "SQ-Map: Efficient layered collision detection and haptic rendering," *IEEE Trans. Vis. Comput. Graph.*, vol. 13, no. 1, pp. 80–93, Jan. 2007.



Athanasios Mademlis was born in Thessaloniki, Greece, in 1980. He received the Diploma degree in electrical and computer engineering in 2004 from Aristotle University of Thessaloniki, where he is currently pursuing the Ph.D. degree in electrical and computer engineering.

Mr. Mademlis is a member of the Technical Chamber of Greece.



Petros Daras (M'06) was born in Athens, Greece, in 1974. He received the Diploma degree in electrical and computer engineering, the M.Sc. degree in medical informatics, and the Ph.D. degree in electrical and computer engineering, all from the Aristotle University of Thessaloniki, Thessaloniki, Greece, in 1999, 2002, and 2005, respectively.

He is a Senior Researcher at the Informatics and Telematics Institute, Thessaloniki. His main research interests include computer vision, search and retrieval of 3-D objects, and medical informatics. He has been involved in more than 15 European and national research projects.

Dr. Daras is a member of the Technical Chamber of Greece.



Apostolos Axenopoulos was born in Thessaloniki, Greece, in 1980. He received the Diploma degree in electrical and computer engineering and the M.S. degree in advanced computing systems from Aristotle University of Thessaloniki, Thessaloniki, Greece, in 2003 and 2006, respectively.

He is an Associate Researcher at the Informatics and Telematics Institute, Thessaloniki. His main research interests include 3-D content-based search and retrieval and bioinformatics.

Mr. Axenopoulos is a Member of the Technical

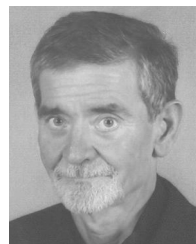
Chamber of Greece.



Dimitrios Tzovaras received the Diploma degree in electrical engineering and the Ph.D. degree in 2-D and 3-D image compression from Aristotle University of Thessaloniki, Thessaloniki, Greece, in 1992 and 1997, respectively.

He is a Senior Researcher in the Informatics and Telematics Institute, Thessaloniki. Previously, he was a Senior Researcher, working on 3-D imaging, at Aristotle University of Thessaloniki. His main research interests include virtual reality, assistive technologies, 3-D data processing, medical image communication, 3-D motion estimation, and stereo and multiview image sequence coding. His involvement with those research areas has led to the co-authoring of more than 35 papers in refereed journals and more than 80 papers in international conferences. He has served as a regular reviewer for a number of international journals and conferences. Since 1992, he has been involved in more than 40 projects in Greece, funded by the European Commission, and the Greek Secretariat of Research and Technology.

Dr. Tzovaras is an Associate Editor of the *EURASIP Journal of Applied Signal Processing* and a member of the Technical Chamber of Greece.



Michael G. Strintzis (M'70–SM'80–F'04) received the Diploma degree in electrical engineering from the National Technical University of Athens, Athens, Greece, in 1967, and the M.A. and Ph.D. degrees in electrical engineering from Princeton University, Princeton, NJ, in 1969 and 1970, respectively.

He then joined the Electrical Engineering Department, University of Pittsburgh, Pittsburgh, PA, where he served as an Assistant Professor (1970–1976) and Associate Professor (1976–1980). Since 1980, he has been a Professor of electrical and computer engineering at the University of Thessaloniki, Thessaloniki, Greece, and, since 1999, Director of the Informatics and Telematics Research Institute, Thessaloniki. His current research interests include 2-D and 3-D image coding, image processing, biomedical signal and image processing, and DVD and Internet data authentication and copy protection.

Dr. Strintzis has served as Associate Editor for the *IEEE TRANSACTIONS ON CIRCUITS AND SYSTEMS FOR VIDEO TECHNOLOGY* since 1999. In 1984, he was awarded one of the Centennial Medals of the IEEE.